International Journal of Steel Structures (2023) 23(2):586–598
https://doi.org/10.1007/s13296-023-00714-6

Online ISSN 2093-6311
Print ISSN 1598-2351

Analysis of Pressure Distribution of the Bolted Joints Based on the Finite Element Method

Sheng-ao Wang[1] · Min Zhu[1] · Fei Wu[1] · Tian-xi Liang[1] · Zhao-qun Shao[1] · Yi-long Liu[1]

Received: 11 March 2022 / Accepted: 12 January 2023 / Published online: 28 January 2023

Abstract
Bolted joints widely exist in the field of the national defense industry. However, its nonlinear stiffness degradation will occur under tangential load which may lead to the reliability reduction. According to Coulomb friction theory, the pressure distribution is the key in the tangential degradation of bolted joints. Therefore, this paper aims to analyze the pressure distribution of bolted joints. Firstly, we established a threaded bolt model and two simplified models. Secondly, the accuracy of the three models describing the contact area is verified, and the influence of preload and material properties on the contact radius is analyzed. Thirdly, we compared the pressure distribution of the three models, and results show that the smooth bolt model is more suitable for pressure analysis. Finally, the accuracy of several different functions to characterize the pressure distribution of bolted joints is analyzed, and results indicated that the Fernlund function is optimal. This paper provides a feasible simplified bolt model for finite element analysis, and the optimal pressure distribution function can be applied in the tangential stiffness degradation modeling.

Keywords Bolted joint · Finite element method · Pressure distribution · Smooth model · Fernlund function

1 Introduction

The dynamics of bolted joints is crucial for the prediction of structural response. A wealth of literature has been published in this field. Argatov et al. (2011) presented mathematical modeling of the non-linear constitutive relation for bolted joints in the framework of the Kragelsky–Demkin theory of rough contact. Gong et al. (2020) proposed a modified Iwan model to represent the nonlinear local slippage behavior and designed several novel thread structures for resisting loosening. Krolo et al. (2016) proposed two different modeling techniques for preloading bolts and the method for solving numerical singularity errors and rigid body motion problems. Segalman et al. (2005, 2009) proposed a modified Iwan model to describe the degradation of bolted joints and verified the accuracy of the model through BMD experiments. However, other scholars have also studied the finite element modeling, pressure distribution, and theoretical model of bolted joints (Marshall et al., 2004; Molinari et al., 2001; Oskouei et al., 2009; Rajaei & Ahmadian, 2014; Sawa et al., 1996; Sherif & Kossa, 1991; Shibahara & Oda, 1972; Wang & Mignolet, 2014; Willner & Gaul, 1995; 李东武 & 徐超., 2017).

The external loads of bolted joint can be decomposed into the tangential load parallel to the interface and the normal load perpendicular to the bolted interface. The tangential load will cause interfacial adhesion, slip, friction, and severe energy dissipation, which is the direct cause of the dynamic degradation and nonlinear behavior. The normal load determines the pressure distribution of bolted joints, indirectly affecting tangential behavior by the friction behavior. Although there is a significant relationship between the two, they are usually studied separately for simplification.

Restoring force under tangential load is mainly provided by friction force, which is related to contact pressure. Therefore, contact pressure is an important factor in the degradation of bolted joints, and the initial preload condition is the starting point. Some scholars have performed relevant experiments, such as pressure-sensitive film experiments (Liao et al., 2016; Pau et al., 2008; 王磊 & 杜瑞, 2013) and ultrasonic experiments (Marshall et al., 2004, 2006). Pau et al.

✉ Min Zhu
min0zhu@163.com

✉ Fei Wu
theone1999@163.com

[1] Naval University of Engineering, Wuhan 430033, China

(2008) designed an ultrasonic test to measure the pressure of the bolted flange by pressure-sensitive film and ultrasonic and compared the experimental results. Wang et al. (2013) performed a pressure-sensitive film experiment and finite element simulation. Results show that finite element simulation is available to analyze the pressure distribution of bolted joints. Marshall et al. (2006) used a nonintrusive ultrasonic technique to quantify the contact pressure distribution in a bolted connection. Results show that the peak contact pressure was found to occur away from the edge of the bolt hole.

Due to additional interface and machining errors, experiments may have low repetition. Therefore, the finite element method is an alternative whose accuracy has been verified by experiments. Liao et al. (2016) established a 2D bolted joint model, and results show that the position of peak interface pressure is between the edge of the bolt hole and the edge of the bolt head. Mangalekar et al. (2016) established a 3D bolted joint model without thread, and results show that the half-cone angle of interfacial pressure distribution is affected by many factors including the plate thicknesses, bolt head diameter, plate material, etc. Fukuoka et al. (2008) proposed an effective mesh generation scheme that can provide helical thread models with accurate geometry to analyze specific characteristics of stress concentrations and contact pressure distributions caused by the helical thread geometry. However, the application of the finite element method in bolted joints is nonsystematic, such as low accuracy and the simplification of the thread with helix.

Therefore, we first make a systematic comparison between the different modeling techniques. Secondly, the influence of preload and other factors on the contact area is analyzed. Finally, the pressure distribution function of bolted joints is analyzed to provide a basis for the stiffness degradation modeling of bolted joints.

2 Modeling Techniques of Bolted Joints

Up to now, the research of bolted joints has mainly focused on two key fields: the stiffness and its response to external load; the geometry and contact pressure distribution on the clamping interface (Gould & Mikic, 1970; Greenwood, 1964; Ito et al., 1979; Lee, et al., 1996; Sawa et al., 1996; Shigley & Mischke, 2001). The pressure distribution is related to bolt clamping, stiffness, fatigue life, and heat transfer capability. There are three main modeling techniques for bolt joints: thread model, smooth model, and MPC model. Among them, the smooth model and MPC model are simplified models.

In the previous modeling of the threaded bolt, researchers usually ignored the thread angle and established the axisymmetric threaded bolt by stacking thread interface geometries. The spiral effect will lead to the loss of symmetry, which may cause changes in the pressure distribution and maximum stress. In recent years, researchers have gradually realized the importance of the spiral effect and begun to use the spiral model (Chen & Shih, 1999; Fukuoka & Nomura, 2008; Zhang et al., 2019). Therefore, we considered the spiral effect of thread angle in the thread bolt modeling.

The finite element model in this paper is built with Abaqus and Hypermesh software, and the simulation is calculated on the server (Windows 10 operating system, 2.30 GHz Intel Xeon Gold 6410 CPU, 192 GB RAM). There are various element types in Abaqus, among which linear-reduced integration elements have the characteristics of accurate displacement results and fast calculation speed and are suitable for contact analysis. Therefore, the linear-reduced integration element C3D8RH is adopted.

Refer to GB/T192 ~ 197-2003 hexagon head bolts (GB/5782-2000) M8 × 36 bolts for the specifications of bolts. The inscribed circle diameter of the bolt head is 13 mm, e is 14.38 mm, the thickness of the bolt head k is 5.3 mm, d_w is 11.63 mm, and the reference value of b is 22 mm, as shown in Fig. 1.

Simplify the bolt and establish the geometric model. The bolt head is a cylinder with a radius of 6.5 mm and a thickness of 5 mm, the total length of the screw is 35 mm, and b is shortened to 7.5 mm to reduce the number of non-contact nodes. The thread profiles are shown in Fig. 2a, b. According to Eq. (1), the pitch P is 1.25 mm. The thread height H is 1.08 mm, and the root arc radius is 0.14 mm. The thickness of the nut is 5 mm, the outer diameter is 13 mm, and the radius of the thread root ρ_n is 0.07 mm.

$$\begin{aligned} &Bolt: \quad \theta_1=\frac{\sqrt{3}\pi}{P}\rho, \quad \theta_2=\frac{7}{8}\pi, \quad \rho \le \frac{\sqrt{3}}{12}P, \quad H=\frac{\sqrt{3}}{2}P \\ &Nut: \quad \theta_1=\frac{\pi}{4}, \quad \theta_2=\pi\left(1-\frac{\sqrt{3}\rho_n}{P}\right), \quad \rho_n \le \frac{\sqrt{3}}{24}P \end{aligned} \tag{1}$$

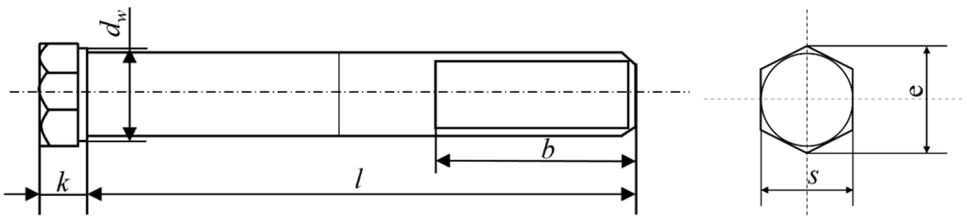

Fig. 1 Schematic diagram of M8 bolt

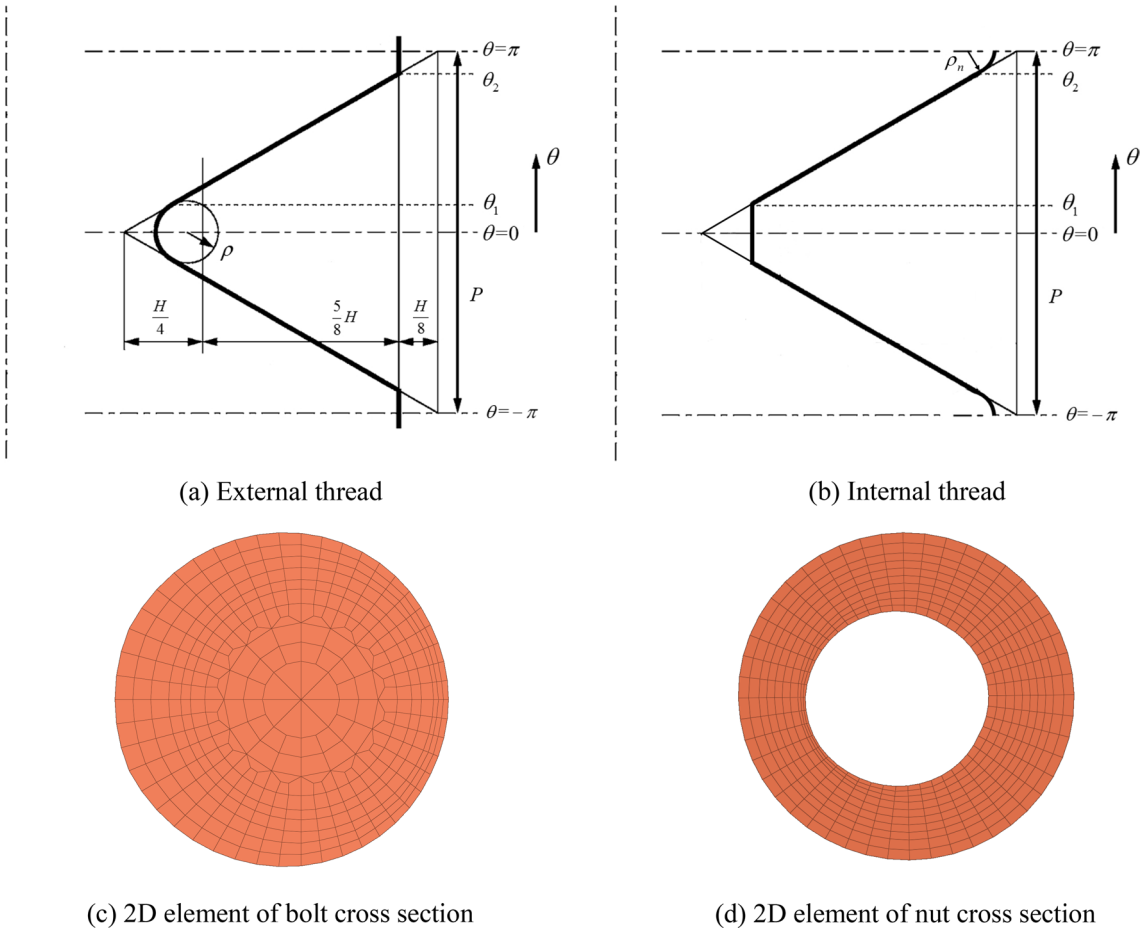

(a) External thread

(b) Internal thread

(c) 2D element of bolt cross section

(d) 2D element of nut cross section

Fig. 2 The thread of bolt and nut

From the perspective of numerical accuracy and calculation efficiency, the mesh at the contact zone shall be refined. 2D cross-section model perpendicular to the axis are established, as shown in Fig. 2c, d. Due to the 2.8473° thread angle, the thread section does not have a central symmetry. The grid size near the thread is smaller, and a grid of about 0.25 mm is adopted.

Translate and rotate the 2D thread element axially at an equal distance and angle within a single pitch, and then the 2D model can be converted to the 3D model through node mapping. Stack the internal and external thread 3D models with single pitch to achieve the complete thread model, as shown in Fig. 3a, b. The grid near the thread is finer, while the grid far from the thread is rougher, which can improve the calculation efficiency and ensure the calculation accuracy.

In the smooth model, the screw is a smooth cylinder with a diameter of 8 mm, and the nut is a hollow cylinder, as shown in Fig. 3c. The contact between the internal and external threads is replaced by imposing constraints on the inner surfaces of the screw and nut.

In the MPC model, the screw is simplified into a beam element, without the structure of bolt head and nut. The contact area of the bolt head and the nut is bound to the ends of the beam through MPC constraints as shown in Fig. 3d.

3 Factors Affecting Contact Area

3.1 Half-Cone Angle of Different Models

When two plates are connected by bolts, the plates will contact within a certain range around the bolts, and separate outside this range (Gould & Mikic, 1970). The half-cone angle is an important parameter to describe the contact range, and the quantitative analysis of the contact area is very important for numerical calculation (Ito et al., 1979; Marshall et al., 2006). Roetscher first proposed the concept of contact cone angle, as shown in Fig. 4. The

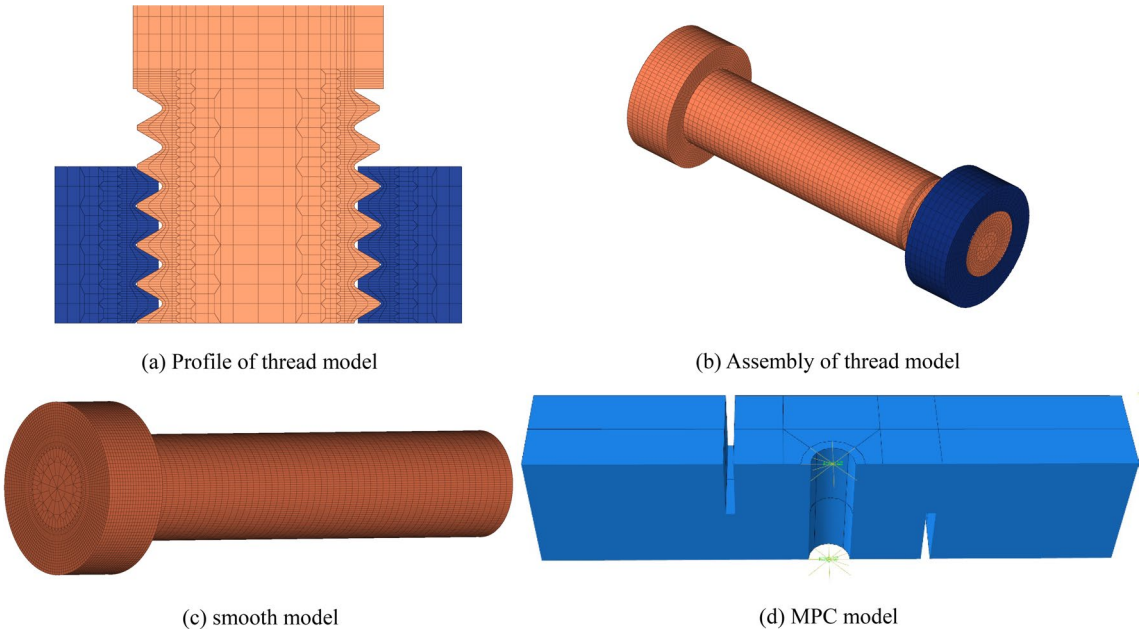

Fig. 3 Finite element models of bolted joints

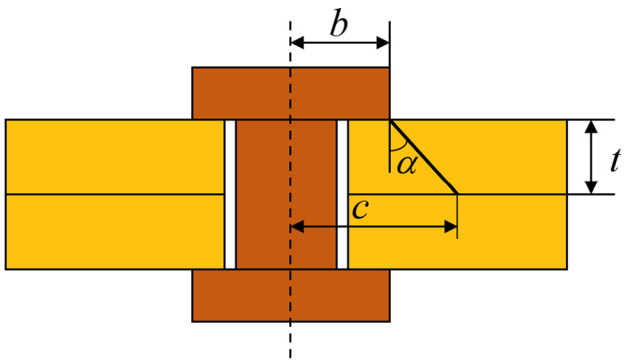

Fig. 4 Contact cone angle of bolt preload structure

relationship between contact radius and plate thickness, bolt head radius, and contact cone angle is as follows:

$$c = b + t\tan\alpha \tag{2}$$

As this research does not aim at specific engineering equipment, there is no specific requirement for preload. A preload force of 1000 N is applied to the bolted plates with a thickness of 15 mm by three bolt models, and the contact radius of the joint surface of the plate is calculated by the finite element method. In static analysis, sufficient constraints must be applied to ensure that no uncertain rigid body displacement occurs at each translational and rotational degree of freedom. Since tangential behavior analysis is not involved in this paper, a friction coefficient of 0.6 is adopted to add sufficient constraints.

Table 1 Contact radius and half-cone angles of different FE models

FEA model	Contact radius (mm)	Half-angles (°)	Deviation from experiment (Ito et al., 1979) (%)
Thread model	16.189	32.858	−8.7
Smooth model	16.195	32.862	−8.7
MPC model	18.959	39.713	10.3

The contact radius and half-cone angles are shown in Table 1. The half-cone angle of the smooth model is consistent with that of the thread model, and the MPC model has a deviation of about 6° with them.

Ito et al. used M8 bolts to measure the half-cone angle with different materials and flange thicknesses, and the angle of the 16 mm plate is 36° (Ito et al., 1979). Considering the deviation caused by the thickness of the plate, the size of the screw hole, and the material parameters,

3.2 Effect of Preload on Contact Radius

The above analysis shows that the results of the three models in simulating the contact area are accurate. Therefore, we applied the smooth model to calculate the factors that affect the contact area under bolt preload. Multiple sets of bolt preloads are applied to the smooth model. The relationship between the preloads and the contact area is shown in Fig. 5.

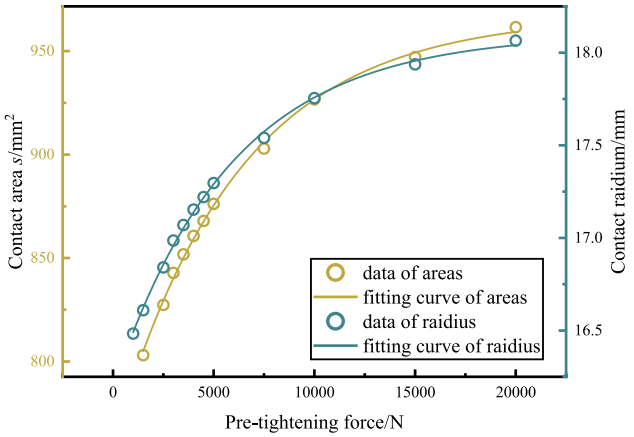

Fig. 5 Preload-contact radius curve

The contact radius increases with the preload, but the increased speed gradually slows down. The preload increased by 20 times from 1000 to 20000 N, and the contact radius increased from 16.195 to 11.4% to 18.046 mm. The increase in preload has little effect on the contact radius. In literature (Liao et al., 2016), the pressure-sensitive film experiment showed that the contact radius was independent on the preload. The difference between the FEA and experimental results may come from the precision of the pressure-sensitive film. Therefore, when the deviation is considered, the pressure-sensitive film experimental results are consistent with the FEA results.

With the increase in preload, the contact area increases nonlinearly, and the increasing speed gradually slows down. It can be characterized by an exponential function as:

$$s = a_0 e^{t_0 F_{pre}} + b_o \tag{3}$$

where, F_{pre} is the bolt preload, a_0, b_0 and t_0 are the fitting parameters($a_0 < 0, t_0 < 0, b_0 > 0$).

The contact radius r can be derived from Eq. (3) as

$$r = \sqrt{\frac{a_0 e^{t_0 F_{pre}} + b_0 + \pi R_{\min}^2}{\pi}} \tag{4}$$

where, $R_{\min}$ is the radius of the hole.

3.3 Effect of Materials on Contact Area

Small changes in the Poisson's ratio and the elastic modulus may occur for different bolt materials. The calculation results of different elastic moduli and Poisson's ratios are shown in Fig. 6. As the increase in elastic modulus, the amplitude of plate warping becomes larger, and the contact area decreases nonlinearly. In the logarithmic coordinate system, there is a linear relationship between the contact area and the elastic modulus, indicating that the elastic modulus and contact area of bolts show power-law characteristics. The contact pressure decreases with the increase of Poisson's ratio, and the Pearson correlation coefficient is -0.98285.

4 Contact Pressure Analysis of Different FEA Models

Under the bolt preload of 1000 N, the initial contact pressure on the inter-plate and bolt head-plate surfaces is shown in Fig. 7. The both pressure peaks appear at the edge of the

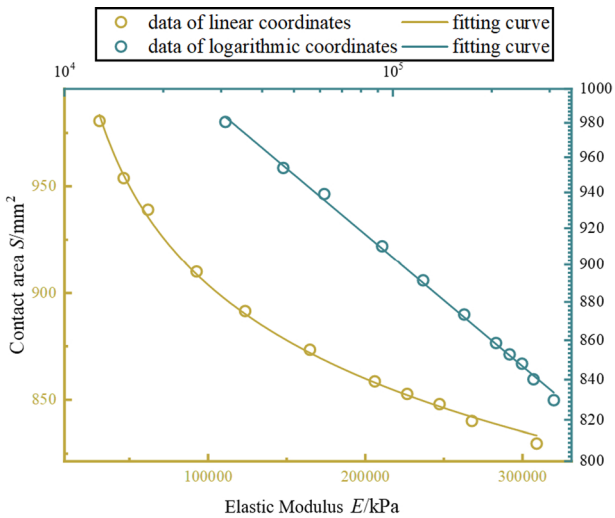

(a) Contact area-elastic modulus curve

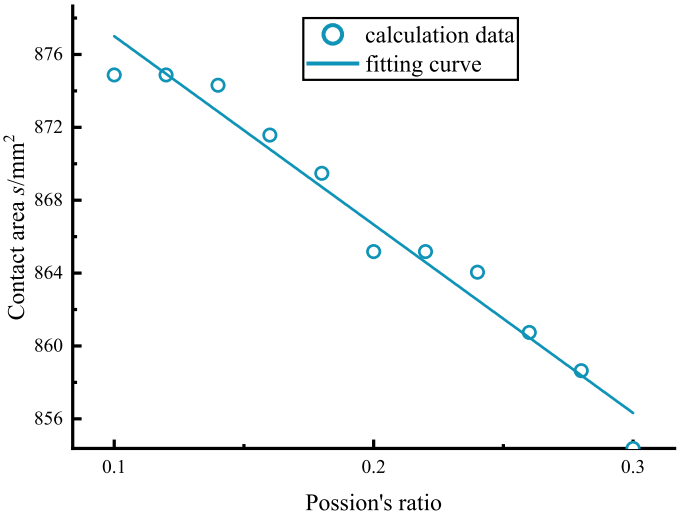

(b) Contact area-possion's ratio curve

Fig. 6 Effect of materials on contact area

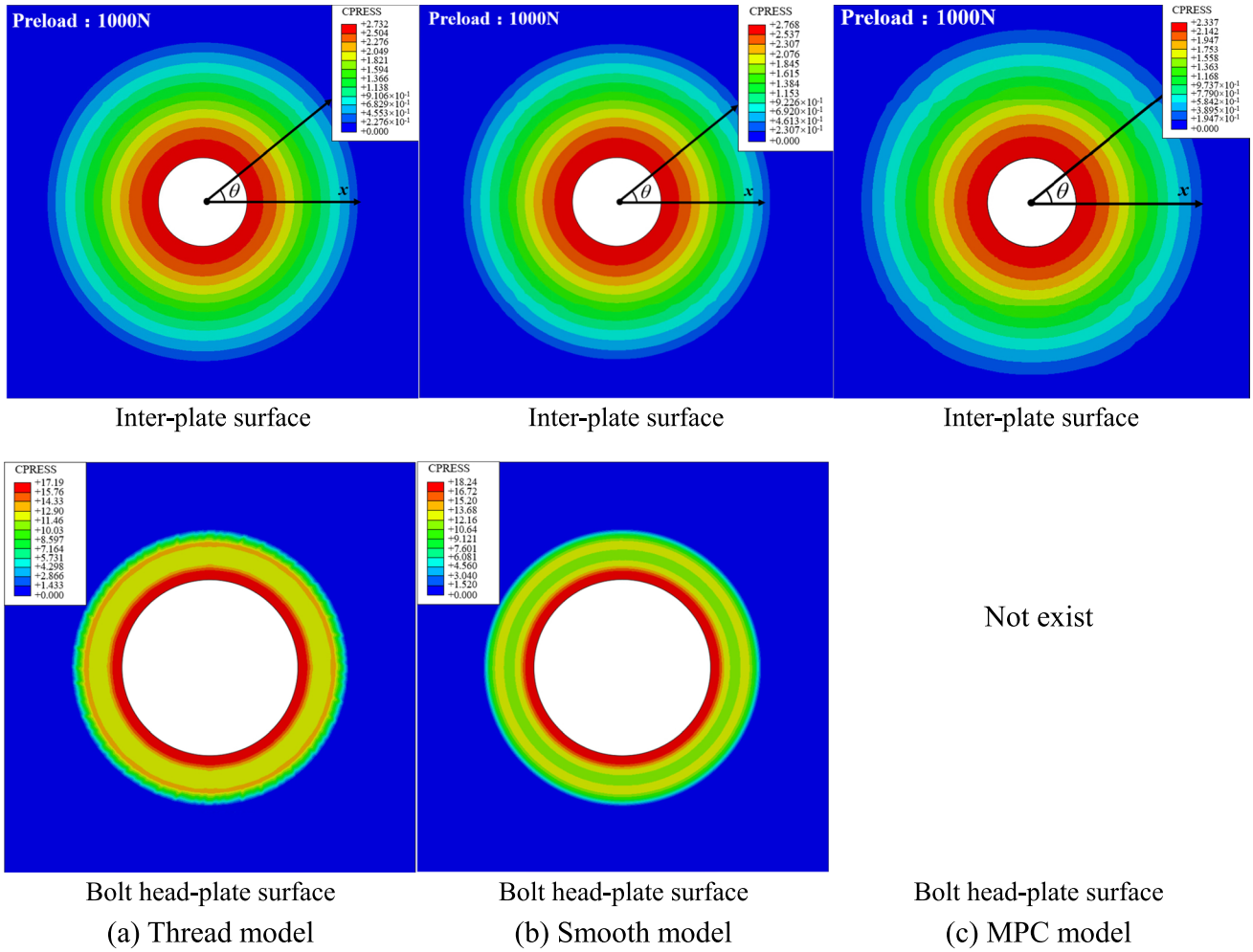

Fig. 7 Contact pressure distribution of the bolted joint

hole, and the pressure on the inter-plate surface decreases monotonically away from the hole. The contact pressure on the bolt head-plate surface reduces non-monotonically. For further analysis, the included angle θ is defined.

To study the influence of the modeling techniques on the pressure distribution, four circular scan paths were determined whose radius is R_{min}, $1.17R_{min}$, $1.33R_{min}$, and $1.5R_{min}$, respectively, where R_{min} is the radius of the screw hole. The variation of the contact pressure with the angle θ on the four scan paths is shown in Fig. 8.

On the inter-plater surface, the contact pressure of the three models at different circumferences are all in harmonic vibrations. The peak appears at $\theta = \pi/2$ and $\theta = 3\pi/2$, and the bottom appears at $\theta = 0$ and $\theta = \pi$. The contact pressure of the smooth model is slightly higher than that of the thread model by about 1.5%~2.5%. The contact pressure of the MPC model is 15%~20% lower than that of the thread model.

On the bolt head-plate surface, the pressure of the thread model is relatively stable, and there is no periodic law. Fluctuation appears on the circumference of $1.5R_{min}$ with an average of 7.647 MPa, and the fluctuation amplitude is 22%. The contact pressure of the smooth model is irrelevant to θ, and the pressure at any angle on the same circle is the same.

Based on the above calculation and analysis, conclusions can be reached as follows:

(1) On the inter-plate surface, the pressure shows a harmonic law for different models, which arises from the geometric boundary.
(2) On the bolt head-plate surface, the pressure stability of the thread model is lower than that of the smooth model, especially on the $1.5R_{min}$ circumference, mainly due to the thread structure.
(3) The relationship between the contact pressure and θ can be expressed by Eq. (5), where P_{pp} is the contact pres-

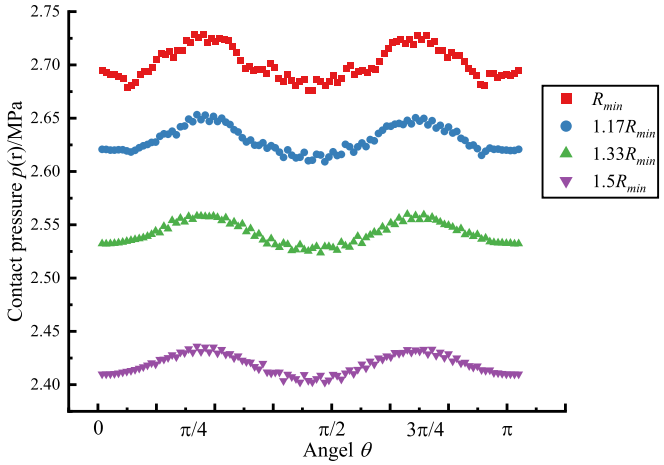

(a1) Inter-plate surface of the thread model

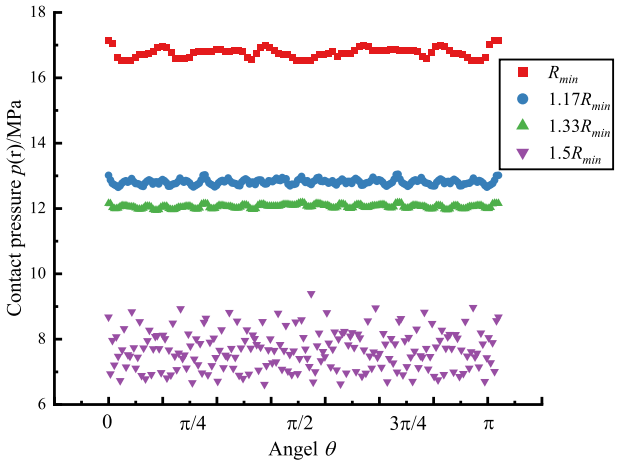

(a2) Bolt head-plate surface of the thread model

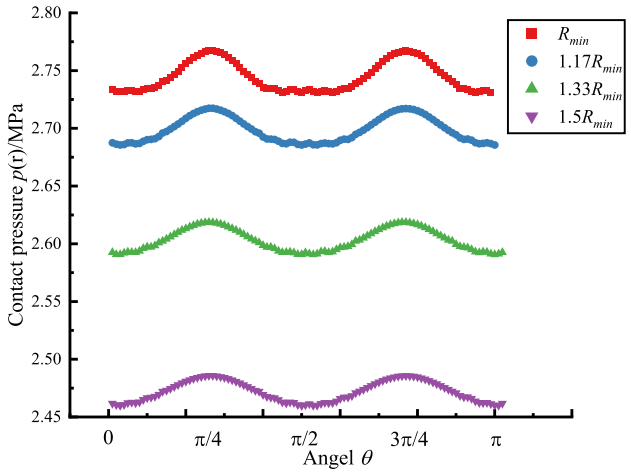

(b1) Inter-plate surface of the smooth model

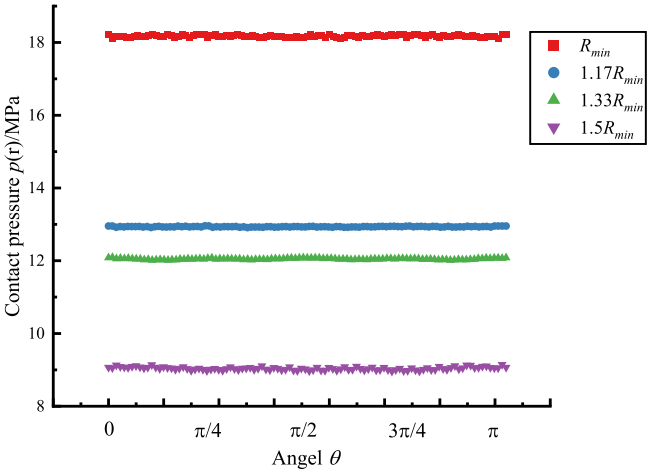

(b2) Bolt head-plate surface of the smooth model

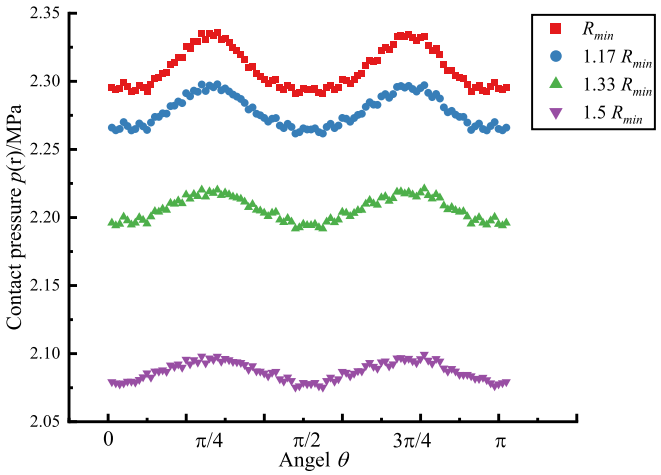

(c) Inter-plate surface of the MPC model

Fig. 8 Contact pressure-angle curve

sure on the inter-plate surface, P_0 is the average contact pressure, and A is the amplitude.

$$P_{pp} = P_0 + A\sin\theta \tag{5}$$

The contact pressure distribution along the radius on the inter-plate surface is shown in Fig. 9a. The contact pressure distributions of the thread model are consistent with that of the smooth model. The MPC model has a larger contact radius and a lower peak pressure, which is quite different from the other two models. Refer to the calculation results of the thread model, following conclusions can be drawn.

(1) MPC model has huge errors, which is not suitable for the contact pressure analysis of bolted joints.

(2) The contact pressure obtained in the previous calculation is in harmonic distribution. Because of the low amplitude, angle θ has little effect on the contact pressure, and the contact pressure is approximately axisymmetric.

The initial contact pressure distribution on the bolt head-plate surface is shown in Fig. 9b. It is necessary to correct the calculation error caused by the element size. The radius of the bolt head is 6.5 mm, while the calculated contact radius is 7.2 mm.

First, the contact radius is corrected by multiplying the coefficient α as

$$\alpha = \frac{r^b_{FEA} - R_{\min}}{S/2 - R_{\min}} \tag{6}$$

where, r^b_{FEA} is the FEA calculated results of contact radius on bolt head-plate surface.

Secondly, the total normal force F^b_N can be obtained by integrating the pressure $p^b_{FEA}(\alpha r)$ over the contact area:

$$F^b_N = \int_{R_{\min}}^{S/2} 2\pi r p^b_{FEA}(\alpha r)dr \tag{7}$$

Finally, multiply $p^b_{FEA}(\alpha r)$ by the coefficient β, and the corrected contact pressure is obtained, as shown in Fig. 9b.

$$\beta = \frac{F_{pre}}{F^b_N} \tag{8}$$

The contact pressure has a non-monotonic decreasing distribution law, and the two peaks appear respectively at and away from the screw hole. The curves of the two models coincide, except for some differences around the screw hole. According to the research results, the smooth model can simulate the contact pressure distribution characteristics of the bolt-threaded connection.

Based on the smooth model, several groups of preload calculations are performed. The relationship between the preload and the peak contact pressure $P_{\max}$ is shown in Fig. 10a. The results show that the peak increases linearly with the increase of bolt pre-tightening force, which is consistent with the experiment results in the literature (Liao et al., 2016).

The contact pressure distribution under the preload of 1000 N, 1500 N, 2500 N, 3500 N, 5000 N, 7500 N, 10000 N, 15000 N, and 20000 N are calculated respectively. The contact pressure distribution along the radius is shown in Fig. 10b, in which the pressure under different preload is significantly different, and the pressure increases as the preload increases.

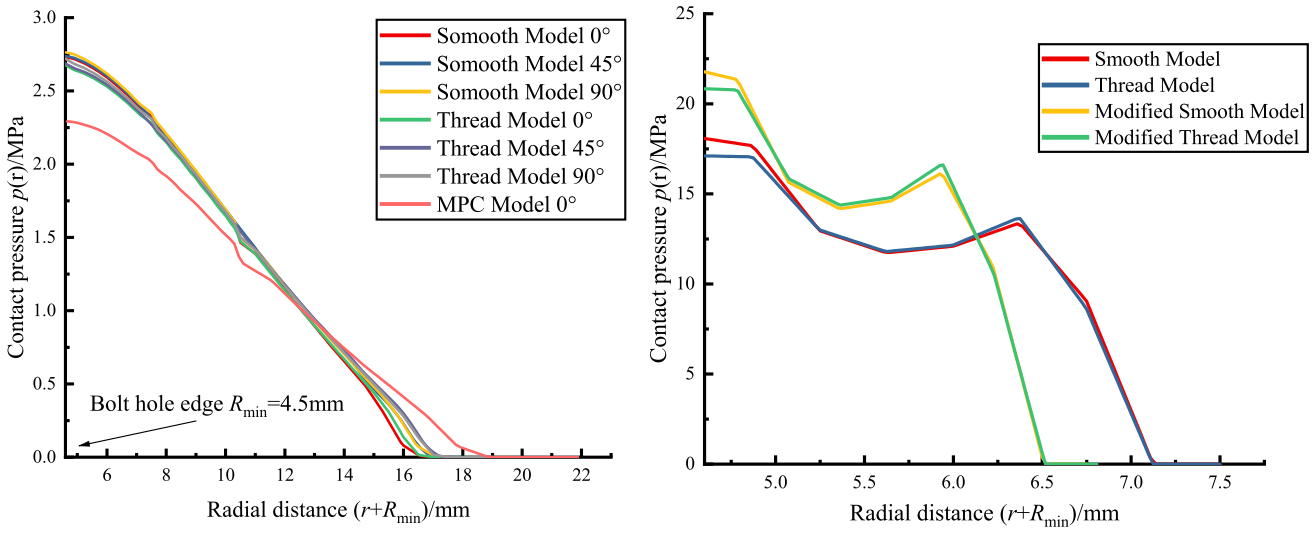

(a) Plate-plate surface

(b) Bolt-head plate surface

Fig. 9 Contact pressure distribution of bolted surfaces

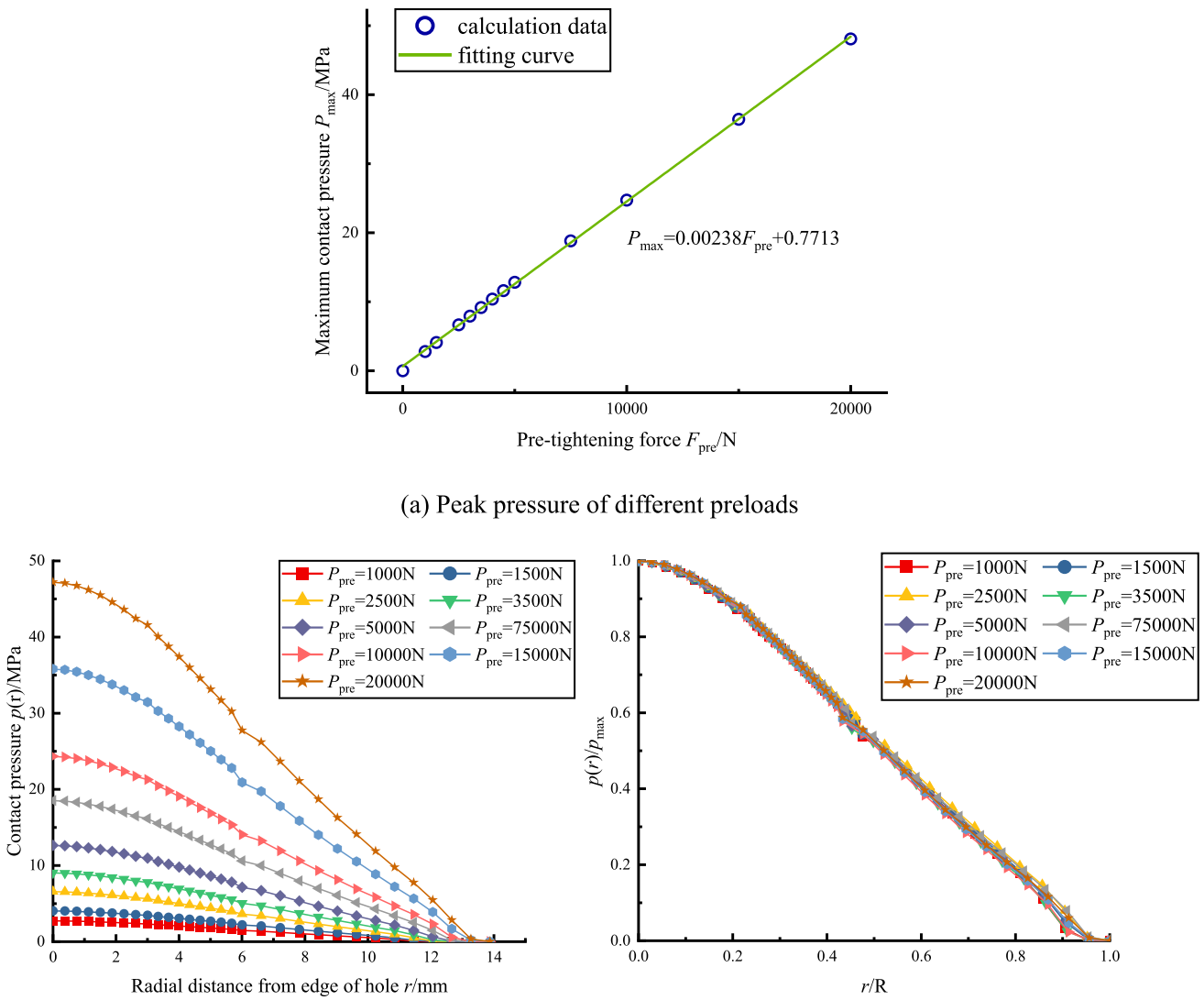

(a) Peak pressure of different preloads

(b) Pressure distribution of different preloads

(c) Normalized pressure distribution curves

Fig. 10 The influence of preload on the contact pressure

Set the ordinate as $p(r)/P_{max}$ and the abscissa as r/R, and normalize the pressure distribution, as shown in Fig. 10c. The normalized curves have high consistency, indicating that the change of pre-tightening force does not change the distribution of the contact pressure. According to the linear relationship between the P_{max} and the preload, it can be concluded that the contact pressure on the same circumference increases linearly with the preload.

5 Analysis of Contact Pressure Distribution Functions

Several distribution functions may be suitable to describe the pressure distribution of bolt bonding surfaces, such as the Fernlund distribution, Hertz distribution, linear distribution, and modified Weibull distribution. Based on Boenick's experimental results and Fernlund's hypothesis of the

pressure distribution, Motosh put forward the Fernlund distribution, as shown in Eq. (9) (Motosh, 1976).

$$p(r) = ar^4 + br^3 + cr^2 + dr + e \quad 0 \le r \le R \tag{9}$$

where, $p(r)$ is the contact pressure; r is the distance from the edge of the bolt hole; a, b, c, d and e are the pressure distribution parameters; R is the length from the contact boundary to the screw hole.

The Fernlund distribution needs to meet the constraints:

$$p(R) = 0, \quad p'(0) = 0,\ p'(R) = 0,\ p''(R) = 0 \tag{10}$$

(1) The contact pressure reaches its peak at $r = 0$, and the contact pressure is 0 at $r = R$;

(2) The first-order gradient of the contact pressure is 0 at $r = 0$ and $r = R$;

(3) The second-order gradient of the pressure at $r = R$ is 0, and the pressure distribution is stable and static.

Combining EqS. (9) and (10), the contact pressure distribution can be simplified as follows.

$$p(r) = \begin{cases} ar^4 - \frac{8}{3}aRr^3 + 2aR^2r^2 - \frac{1}{3}aR^4 & 0 \le r \le R \\ 0 \quad else \end{cases} \tag{11}$$

Since P_{max} is always greater than zero, the constraint $a < 0$ is generated. In this paper, mm-10^3 kg-s-MPa is adopted as the unified system of units. Thus, the dimension of a is MPa/mm^4.

The total normal pressure at the contact surface can be obtained by integrating the contact pressure over the area, such as Eq. (12).

$$N_0 = \int_0^R 2\pi(r + R_{min})p(r)dr = -\frac{\pi aR^5\left(R + 4R_{min}\right)}{15} \tag{12}$$

Weibull distribution is a statistical distribution model. Mantelli conducted a total of 30 experiments with six kinds of material and five torques. Among them, the experimental group made of 304 stainless steel and 304 stainless steel, under the preloads of 1624 N, 3247 N, 6672 N, and 12233 N showed a pressure increase at the edge of the bolt hole (Mantelli et al., 2010). In addition to the Mantelli experiment, Marshall also measured the pressure distribution of the bolt pre-tightening structure by ultrasonic method. The results showed that the peak appeared between the bolt head and the screw hole. The research results of Ziada and Liao based on the 2D finite element model show that the peak pressure appears outside the screw hole(Liao et al., 2016).

Weibull distribution can characterize the local increase of the contact pressure around the hole. By multiplying the parameter ρ, the integral of the contact pressure in the contact area can agree with the normal pressure. The revised Weibull distribution is

$$p(r) = \rho\frac{\beta}{\eta}\left(\frac{r}{\eta}\right)^{\beta-1}e^{-(r/\eta)^{\beta}} \tag{13}$$

where, β,η and ρ are the parameters to be identified.

The Hertz distribution simplifies the rough surface contact to the contact between the elastic asperities and the rigid plate. In general, the statistical summation model is the main application scenario of the Hertz distribution, regardless of the coupling effect. Therefore, the Hertz pressure distribution cannot represent the pressure distribution characteristics of the bolted joint. As shown in Fig. 11a, the Hertz distribution shows poor performance in describing the pressure on the inter-plate surface.

Linear distribution is a simplified assumption of idealization and linearization of contact pressure distribution. Although the distribution function is very simple, Fig. 11b shows that it still has a good representation effect. However, the linear distribution function has the limitation in describing the gradient characteristics at both ends of the pressure distribution curve, which is the main error source.

As shown in Fig. 11c, the peak value of the modified Weibull distribution does not appear at $r=0$, and the error between the two ends of the theoretical curve and the results of finite element analysis is large. At first, Weibull distribution was proposed to characterize the increase of contact pressure around the screw hole, but the FEA results do not support this precondition. In addition, the FEA results and some scholars' experimental results also support the calculation results. Mangalekar obtained the location of the peak pressure by the FEA method and pointed out that the peak pressure appeared at the bolt hole (Ramdas & Dawari 2016). Sawa showed that the contact pressure decreases monotonously through pressure-sensitive films and probes, ultrasonic experiments, and theoretical analysis (Sawa et al., 1996). Because the local pressure increase in the Mantelli experiment only exists in specific experimental groups, and the pressure-sensitive film is not accurate enough, inconsistent results between different experimental groups can be invalid. The FEA calculation supporting local pressure increase is based on a rough and simplified 2D model, and its reliability is lower than that of later scholars' finer model. Therefore, the modified Weibull distribution is not suitable to characterize the pressure distribution of bolted joints, and the local increment of experimental and simulation results is due to experimental errors and inaccurate modeling methods.

The fitting effect of Fernlund distribution is shown in Fig. 11d, which can represent the gradient changes at both ends of the curve, and has a good fitting effect. However, through local enlargement, it can be found that there is a poor fitting effect at the contact boundary. To further study the error of Fernlund distribution on contact boundary, a large plate model with the ratio of plate width to bolt

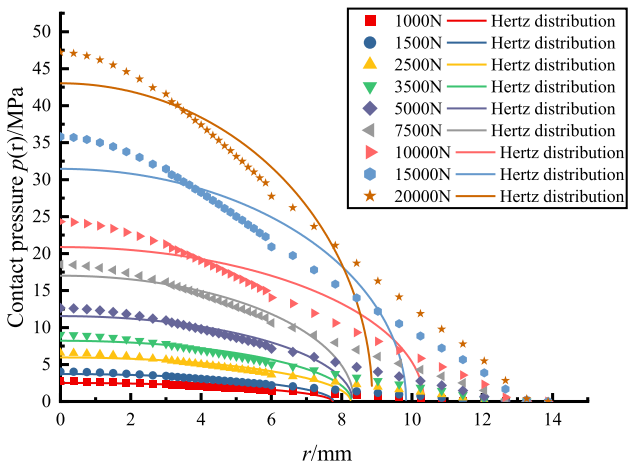

(a) Hertz distribution

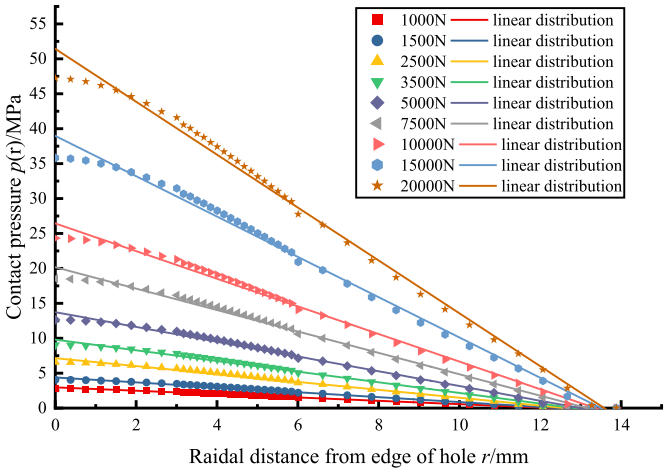

(b) Linear distribution

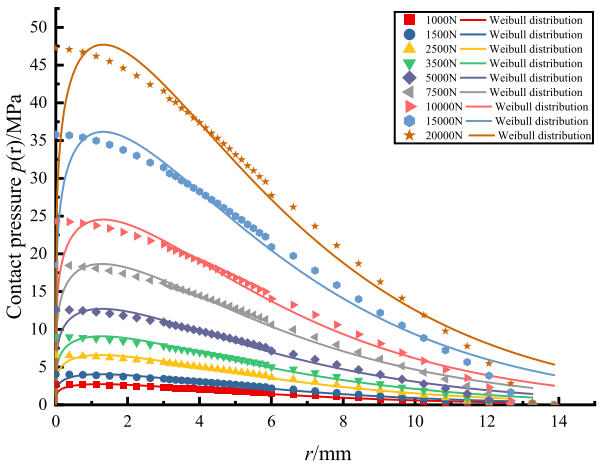

(c) Weibull distribution

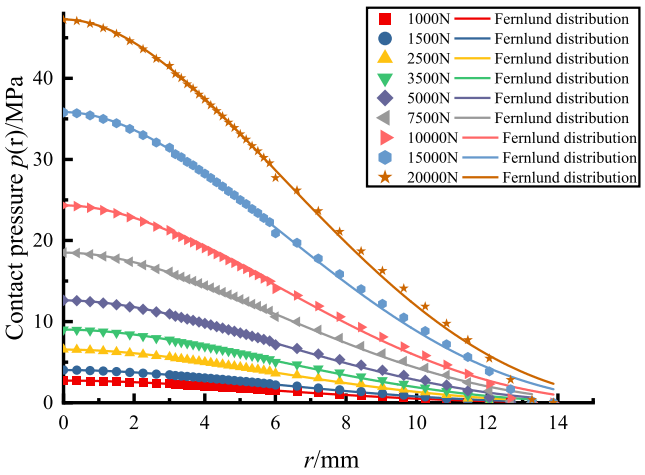

(d) Fernlund distribution

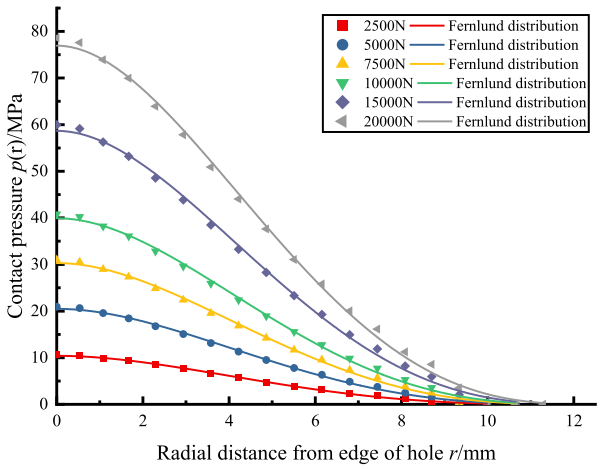

(e) Fernlund distribution of an infinite plate

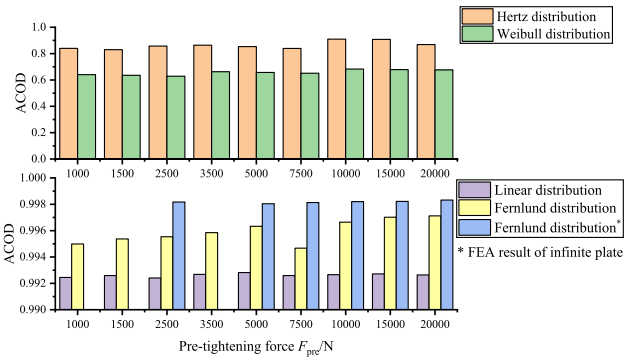

(f) Adjusted coefficient of determination

Fig. 11 Comparison of contact pressure theory

diameter of 10 was established to approximate an infinite plate. The calculated contact pressure distribution and Fernlund fitting curves are shown in Fig. 11e. The Fernlund distribution can ideally describe the pressure distribution characteristics of large plate-bolt diameter ratios. Thus, the pressure error at the contact boundary in Fig. 11d is caused by the geometry boundary.

The adjusted coefficients of determination of the above four distributions are shown in Fig. 11f. The coefficients of linear distribution and the Fernlund distribution are the highest, and Fernlund distribution has the best effect.

6 Conclusion

In this paper, three bolted joint models are established. The model applicability, factors affecting the contact radius, pressure distribution with angle and distance, and the applicability of different distribution theories are studied, respectively. The following conclusions are obtained.

(1) In the contact analysis of the initial preload, the simplification of the bolted joint model will lead to different degrees of calculation deviations. The calculation result of the smooth model is the closest to that of the thread model. The smooth model is more suitable for the contact analysis of bolted joints for its easier modeling and higher efficiency.
(2) The elastic modulus, Poisson's ratio, and the applied preload have little influence on the contact radius. It's hard to pick up such a small effect in the experiment.
(3) The contact pressure on the inter-plate surface shows harmonic characteristics. Because the amplitude is small, it can be neglected when analyzing the radial pressure distribution. The pressure on the inter-plate surface decreases monotonically, and there is a local increase at the bolt head-plate surface.
(4) With the increase in the preload, the contact pressure increases significantly. The normalization results show that the increase in the preload changes the amplitude, and the distribution rule is unchanged.
(5) Among the four distribution functions, linear distribution and Fernlund distribution can characterize the distribution characteristics of contact pressure, while Weibull distribution and Hertz distribution are poor. Compared with the linear distribution, the Fernlund distribution can better represent the gradient of the contact pressure at both ends. When the plate is large enough, the effect of the Fernlund distribution can be significantly improved.

References

Argatov, I. I., & Butcher, E. A. (2011). On the Iwan models for lap-type bolted joints. *International Journal of Non-Linear Mechanics, 46*(2), 347–356.

Chen, J.-J., & Shih, Y.-S. (1999). A study of the helical effect on the thread connection by three dimensional finite element analysis. *Nuclear Engineering and Design, 191*(2), 109–116.

Fukuoka, T., & Nomura, M. (2008). Proposition of helical thread modeling with accurate geometry and finite element analysis. *Journal of Pressure Vessel Technology*. https://doi.org/10.1115/1.2826433

Gong, H., Liu, J., & Ding, X. (2020). Thorough understanding on the mechanism of vibration-induced loosening of threaded fasteners based on modified Iwan model. *Journal of Sound and Vibration, 473*, 115238.

Gould, H. H., & Mikic, B. B. (1972). Areas of contact and pressure distribution in bolted joints. *Journal of Engineering for Industry, 94*(3), 864–870. https://doi.org/10.1115/1.3428263

Greenwood, J. (1964). The elastic stress produced in the mid plane at a slab by pressure applied symmetrically at its surface. *Mathematical Proceedings of the Cambridge Philosophical Society, 60*, 159–169.

Ito, Y., Toyoda, J., & Nagata, S. (1979). Interface pressure distribution in a bolt-flange assembly. *Journal of Mechanical Design, 101*(2), 330–337.

Krolo, P., Grandić, D., & Bulić, M. (2016). The guidelines for modelling the preloading bolts in the structural connection using finite element methods. *Journal of Computational Engineering, 2016*, 4724312.

Lee, S., Song S., Moran K. P. et al. (1996). Analytical modeling of thermal resistance in bolted joints.

Liao, J. P., Yu, D. W., & Feng, P. F. (2016). Factors affecting contact pressure distribution on bolted joint interface. *Key Engineering Materials, 693*, 126–133.

Mangalekar, R., Ramdas, C., Dawari, B. (2016). Study of interfacial pressure distribution for preloaded bolted connection. In: *Proceedings of the international conference on communication and signal processing* (ICCASP 2016), vol. 2016: pp. 265–270.

Mantelli, M., Milanez, F., Pereira, E., et al. (2010). Statistical model for pressure distribution of bolted joints. *Journal of Thermophysics and Hear Transfer, 24*, 432–437.

Marshall, M. B., Lewis, R., Drinkwater, B. W., et al. (2004). An ultrasonic approach for contact stress mapping in machine joints and concentrated contacts. *The Journal of Strain Analysis for Engineering Design, 39*(4), 339–350.

Marshall, M. B., Lewis, R., & Dwyer-Joyce, R. S. (2006). Characterisation of contact pressure distribution in bolted joints. *Strain, 42*(1), 31–43.

Molinari, J. F., Ortiz, M., Radovitzky, R., et al. (2001). Finite-element modeling of dry sliding wear in metals. *Engineering Computations, 18*(3/4), 592–610.

Motosh, N. (1976). Determination of joint stiffness in bolted connections. *Journal of Engineering for Industry, 98*(3), 858–861.

Oskouei, R. H., Keikhosravy, M., & Soutis, C. (2009). Estimating clamping pressure distribution and stiffness in aircraft bolted joints by finite-element analysis. *Proceedings of the Institution of Mechanical Engineers, Part g: Journal of Aerospace Engineering, 223*(7), 863–871.

Pau, M., Baldi, A., & Leban, B. (2008). Visualization of contact areas in bolted joints using ultrasonic waves. *Experimental Techniques, 32*(4), 49–53.

Mangalekar, R., Ramdas, C., & Dawari, B. (2016). Study of interfacial pressure distribution for preloaded bolted connection. In: *International Conference on Communication and Signal Processing 2016* (ICCASP 2016) (pp. 265-270). Atlantis Press.

Rajaei, M., & Ahmadian, H. (2014). Development of generalized Iwan model to simulate frictional contacts with variable normal loads. *Applied Mathematical Modelling, 38*(15), 4006–4018.

Sawa, T., Kumano, H., & Morohoshi, T. (1996). The contact stress in a bolted joint with a threaded bolt. *Experimental Mechanics, 36*(1), 17–23.

Segalman, D. J. (2005). A four-parameter iwan model for lap-type joints. *Journal of Applied Mechanics, 72*(5), 752–760.

Segalman, D. J., & Gregory, D. L. (2009). *Handbook on dynamics of jointed structure*. Sandia Laboratory.

Sherif, H., & Kossa, S. (1991). Relationship between normal and tangential contact stiffness of nominally flat surfaces. *Wear, 151*, 49–62.

Shibahara, M., & Oda, J. (1972). On clamping stiffnesses of abutments in bolted joints. *Bulletin of JSME, 15*(79), 104–115.

Shigley, J. E., & Mischke, C. R. (2001). *Mechanical Engineering Design, 6th end*. McGraw-Hill.

Wang, X. Q., & Mignolet, Marc P. (2014). Stochastic Iwan-type model of a bolted joint: Formulation and identification. *Dynamics of Coupled Structures.* Springer International Publishing.

Willner, K., & Gaul, L. (1995). A penalty approach for contact description by FEM based on interface physics conference contribution. *Computational Methods in Contact Mechanics, II*, 257–264.

Zhang, M., Zeng, D., Lu, L., et al. (2019). Finite element modelling and experimental validation of bolt loosening due to thread wear under transverse cyclic loading. *Engineering Failure Analysis, 104*, 341–353.

李东武, 徐超 (2017). 考虑法向载荷变化的Iwan模型及其特性分析. 哈尔滨工业大学学报, 49(10): 138–144.

王磊, 杜瑞, 金涛, et al. (2013). 螺钉连接固定结合面匹配设计研究. 西安交通大学学报, 47(07): 62–67.